Engineering sticky superomniphobic surfaces on transparent and flexible PDMS substrate

Renaud Dufour, Maxime Harnois, Yannick Coffinier, Vincent Thomy, Rabah Boukherroub, Vincent Senez

Engineering Sticky Superomniphobic Surfaces on Transparent and Flexible PDMS Substrate

Renaud Dufour,[†,‡] Maxime Harnois,[†] Yannick Coffinier,[‡] Vincent Thomy,[†] Rabah Boukherroub,[‡] and Vincent Senez*[,†]

[†]*University Lille Nord de France, Institute of Electronics, Microelectronics and Nanotechnology (IEMN, UMR 8520), Cité Scientifique, Avenue Poincaré, BP 60069, 59652 Villeneuve d'Ascq, France, and* [‡]*Interdisciplinary Research Institute (IRI, USR 3078), Parc de la Haute Borne, 50 Avenue de Halley, BP 70478, 59658 Villeneuve d'Ascq, France*

Following the achievement of superhydrophobicity which prevents water adhesion on a surface, superomniphobicity extends this high repellency property to a wide range of liquids, including oils, solvents, and other low surface energy liquids. Recent theoretical approaches have yield to specific microstructures design criterion to achieve such surfaces, leading to superomniphobic structured silicon substrate. To transfer this technology on a flexible substrate, we use a polydimethylsiloxane (PDMS) molding process followed by surface chemical modification. It results in so-called sticky superomniphobic surfaces, exhibiting large apparent contact angles ($> 150°$) along with large contact angle hysteresis ($> 10°$). We then focus on the modified Cassie equation, considering the 1D aspect of wetting, to explain the behavior of droplets on these surfaces and compare experimental data to previous works to confirm the validity of this model.

Introduction

The interest for liquid repellent surfaces has extensively increased during the past decade, motivated by a wide range of potential applications: antifouling and nonadhesive surfaces, microfluidics, energy conversion and conservation,[1] and underwater applications.[2]

Observation of natural surfaces has been of great importance for the understanding of wetting on textured surfaces. A look at particular plant leaves reveals different mechanisms leading to high water repellency.[3,4] The most known is the so-called "lotus effect", in reference to the superhydrophobic lotus leaf, which exhibits contact angle (CA) with water as large as 170° and small contact angle hysteresis (CAH). The lotus belongs to a first type of plants looking macroscopically smooth, but presenting hierarchical structures at micro and nano scales. A second type of leaves, such as Lady's Mantle, are covered with multi cellular hairs, a structure which also results in superhydrophobic properties. On these hairy or microstructured surfaces, water droplets easily roll off, leading to a self-cleaning effect.

Analysis of these natural surfaces, along with various theoretical and experimental studies of surface wettability, point out two main parameters responsible for liquid repellency. First a low surface energy material (or coating) should be used (in other words, it should be initially hydrophobic). Second, to increase the hydrophobic character, the surface should be micro and/or nano structured. On such textured surfaces, droplets sit on a patchwork of solid and air. This induces a reduction in solid−liquid contact, responsible for superhydrophobic properties.

From these findings, many artificial surfaces have been developed. Some of them mimic the lotus leaf characteristics, with more or less ordered micro and/or nano structures: silicon pillars,[5] molded polymers,[6] fractal surfaces,[7] nanoparticles coatings,[8] and so one. Others are more similar to hairy plants, made for instance of silicon nanowires or carbon nanotubes.[9−12]

Following the achievement of highly water repellent surfaces, a new emerging and challenging issue is to extend this concept to design superomniphobic surfaces. The latter should present similar characteristics, i.e., high CA ($\theta > 150°$) and low CAH ($\Delta\theta < 10°$) not only with water but also with a wide range of liquids such as oils and organic solvents. These surfaces are also called superoleophobic or superhygrophobic. However this property is more complicated to achieve since these low surface tension liquids tend to wet most of the natural or artificial superhydrophobic surfaces. Indeed, despite their high water repellency, plant leaves are not able to repel oil droplets, which spread into the asperities of microstructures. To overcome this problem, theoretical considerations have led to specific design criterion preventing liquid penetration between microstructures.[13] This criterion involves geometries presenting re-entrant curvatures (or overhangs), which enable contact line pining to keep a composite

*To whom correspondence should be addressed. Tel: +33 3 20 19 78 55. Fax: +33 3 20 19 78 84. E-mail: vincent.senez@isen.fr.

(1) Nosonovsky, M.; Bhushan, B. *Curr. Opin. Colloid Interface Sci.* **2009**, *14*, 270–280.
(2) Marmur, A. *Langmuir* **2006**, *22*, 1400–1402.
(3) Koch, K.; Bhushan, B.; Barthlott, W. *Progress Mater. Sci.* **2009**, *54*, 137–178.
(4) Otten, A.; Herminghaus, S. *Langmuir* **2004**, *20*, 2405–2408.
(5) Bico, J.; Marzolin, C.; Quere, D. *Europhys. Lett.* **1999**, *47*, 220–226.
(6) Cortese, B.; D'Amone, S.; Manca, M.; Viola, I.; Cingolani, R.; Giuseppe, G. *Langmuir* **2008**, *24*, 2712–2718.
(7) Shibuichi, S.; Yamamoto, T.; Onda, T.; Tsujii, K. *J. Colloid Interface Sci.* **1998**, *208*, 287–294.
(8) Zimmermann, J.; Reifler, F. A.; Fortunato, G.; Gerhardt, L. C.; Seeger, S. *Adv. Funct. Mater.* **2008**, *18*, 3662–3669.
(9) Lapierre, F.; Brunet, P.; Coffinier, Y.; Thomy, V.; Blossey, R.; Boukherroub, R. *Faraday Discuss.* **2010**, DOI: 10.1039/b925544c.
(10) Lapierre, F.; Thomy, V.; Coffinier, Y.; Blossey, R.; Boukherroub, R. *Langmuir* **2009**, *25*, 6551–6558.
(11) Verplanck, N.; Galopin, E.; Camart, J.-C.; Thomy, V.; Coffinier, Y.; Boukherroub, R. *Nano Lett* **2007**, *7*, 813–817.
(12) Brunet, P.; Lapierre, F.; Thomy, V.; Coffinier, Y.; Boukherroub, R. *Langmuir* **2008**, *24*, 11203–11208.
(13) Tuteja, A.; Choi, W.; Mabry, J. M.; McKinley, G. H.; Cohen, R. E. *Proc. Natl. Acad. Sci.* **2008**, *105*, 18200–18205.

interface under the drop. The same underlying mechanism is used to make superhydrophobic surfaces from a hydrophilic substrate.[14,15] Such surfaces have been demonstrated with so-called microhoodoos and nanonails obtained by silicon etching processes[13,16] and also with inverted trapezoidal structures in PDMS involving a diffusive photolithography technique.[17] Apart from these particular geometries, superomniphobic surfaces have also been obtained by more randomly organized nanostructures involving the same mechanism: nanoparticles and nanowires deposition on textile fibers,[18,19] electropolymerization,[20] electroless etching method[21] or silica spheres stacking layers.[22]

Most of these surfaces have been realized on solid substrates or with specific fabrication processes. However, different applications such as liquid repellent coatings or flexible microfluidic devices require flexible superomniphobic surfaces. In this study, we propose an original method based on a single lithography-step approach associated with a polydimethylsiloxane (PDMS) molding process to prepare sticky superomniphobic, flexible, and transparent surfaces. Sticky surfaces are surfaces with a high CA (> 150°) and a high CAH (> 10°). The first part of this paper summarizes some basics of wetting, considering the two models of Wenzel and Cassie−Baxter. We then focus on the particular design criterion needed to achieve superomniphobicity and also on the 1D aspect of wetting, essential for the understanding of CAH on textured surfaces. After a description of the technological process, experimental static, advancing and receding apparent contact angles (ACA) are reported for 6 different liquids over 5 samples presenting distinct geometries. Finally, the results are compared to the 1D wetting model in order to obtain a qualitative estimation of both contact line deformation and explanation of the observed CAH.

Design Criteria to Achieve Superomniphobicity. Wettability on nonplanar surfaces is commonly described by two models. The first one from Wenzel relates CA variation to surface roughness[23] and is described by eq 1, where θ is the Wenzel ACA, r the surface roughness, and θ_Y the Young angle, which is the equilibrium CA on the corresponding smooth surface given by eq 2.[24] γ_{SV}, γ_{SL}, and γ_{LV} refer to solid−vapor, solid−liquid, and liquid−vapor interfacial tensions, respectively. On the plane surface, θ_Y is comprised between the advancing and receding angles, respectively noted θ_A and θ_R.

$$\cos\theta_W^* = r\cos\theta_Y \tag{1}$$

$$\cos\theta_Y = \frac{\gamma_{SV}-\gamma_{SL}}{\gamma_{LV}} \tag{2}$$

The second model from Cassie and Baxter considers air pockets trapped between liquid and solid surface, leading to the so-called Fakir state. This configuration is described by eq 3, where θ_C^* is the Cassie ACA, Φ_S the fraction of solid−liquid interface below the drop, and θ_Y the Young CA.

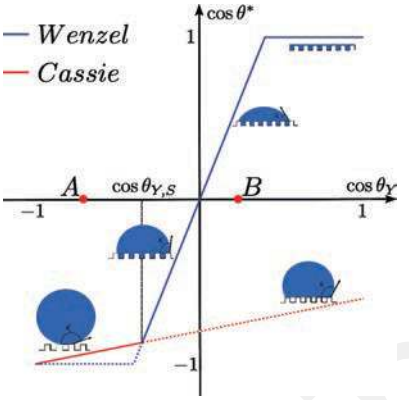

Figure 1. ACA cosine as a function of the Young angle cosine for the Cassie model (red line) and the Wenzel configuration (blue line). Continuous and dotted lines correspond to stable and metastable states, respectively.[27].

$$\cos\theta_C^* = \Phi_S(1+\cos\theta_Y)-1 \tag{3}$$

As far as liquid repellency is concerned, the Cassie state is preferable for two reasons: (i) it enables large ACA even from small Young angle and (ii) it reduces liquid−solid contact area and thus CAH. However, although Cassie state is relatively easy to obtain with water, this is not the case with low surface tension liquids, which generally prefer the Wenzel configuration.

For a given surface (r and Φ_S fixed), these two models are not energetically equivalent.[25] Equalizing eqs 1 and 3 leads to eq 4 where the threshold Young angle $\theta_{Y,S}$ delimitates stable and metastable states.[26] For $\theta_Y < \theta_{Y,S}$, the lower energetic state corresponds to the Wenzel configuration, whereas the Cassie state is more stable for $\theta_Y > \theta_{Y,S}$

$$\cos\theta_{Y,S} = \frac{\Phi_S-1}{r-\Phi_S} > 90° \tag{4}$$

These behaviors are summarized in Figure 1 where the Wenzel model is depicted in blue and Cassie in red. Continuous and dotted lines correspond to stable and metastable states, respectively. This representation gives the ACA as a function of the Young angle for a given surface (parameters Φ and r fixed, resulting in a fixed $\theta_{Y,S}$). Considering a water droplet, the Young angle can be made larger than $\theta_{Y,S}$ on usual hydrophobic materials, which corresponds to point A in Figure 1. Consequently, it enables a stable Cassie configuration. Furthermore, for an oil or an organic solvent, $\theta_Y < 90° < \theta_{Y,S}$ even on the lowest surface energy materials. This corresponds to point B in Figure 1. In this case, the Wenzel state is stable (continuous blue line) and the Cassie one is metastable (dotted red line). To reach this metastable Cassie state, the surface must be able to sustain a composite interface fulfilling locally the Young condition at the top of the microstructures. This is possible only if using microstructures with overhangs,[25] which enable contact line pining on the upper part for $\theta_Y > 90°$ and on the lower part for $\theta_Y < 90°$ (Figure 4). This specific design criterion has been used to obtain superomniphobic surfaces on PDMS.

1D Aspect of Wetting. Numerous studies[28−31] demonstrate that wetting is not only a 2D phenomenon, but a 1D aspect must

(14) Liu, J.-L.; Feng, X.-Q.; Wang, G.-F.; Yu, S.-W. *J. Phys.: Condens. Matter* **2007**, *19*, 356002.
(15) Cao, L. L.; Hu, H. H.; Gao, D. *Langmuir* **2007**, *23*, 4310–4314.
(16) Ahuja, A.; Taylor, J. A.; Lifton, V.; Sidorenko, A. A.; Salamon, T. R.; Lobaton, E. J.; Kolodner, P.; Krupenkin, T. N. *Langmuir* **2008**, *24*, 9–14.
(17) Im, M.; Im, H.; Lee, J.-H.; Yoon, J.-B.; Choi, Y.-K. *Soft Matter* **2010**, *6*, 1401–1404.
(18) Choi, W.; Tuteja, A.; Chhatre, S.; Mabry, J. M.; Cohen, R. E.; McKinley, G. H. *Adv. Mater.* **2009**, *21*, 2190–+.
(19) Brewer, S. A.; Willis, C. R. *Appl. Surf. Sci.* **2008**, *254*, 6450–6454.
(20) Darmanin, T.; Guittard, F. *J. Mater. Chem.* **2009**, *19*, 7130–7136.
(21) Nguyen, T. P. N.; Brunet, P.; Coffinier, Y.; Boukherroub, R. *Langmuir*, **2010**, in press.
(22) Hsieh, C. T.; Wu, F. L.; Chen, W. Y. *Mater. Chem. Phys.* **2010**, *121*, 14–21.
(23) Wenzel, R. N. *Ind. Eng. Chem.* **1936**, *28*, 988–994.
(24) Young, T. *Philos. Trans. R. Soc. London* **1805**, *95*, 65–87.
(25) Herminghaus, S. *Europhys. Lett.* **2000**, *52*, 165–170.
(26) Bico, J.; Thiele, U.; Quere, D. *Colloids Surf. A-Physicochem. Eng. Aspects* **2002**, *206*, 41–46.

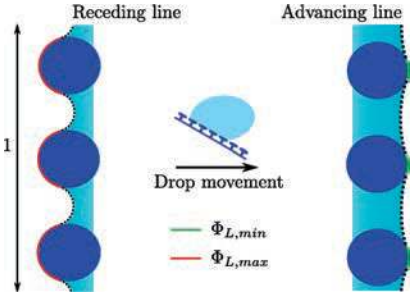

Figure 2. Variation of the linear fraction parameter Φ_L considering the advancing or receding contact line. Φ_L reaches its maximum and minimum values for the receding and advancing line, respectively.

be considered. Contact angle does not depend on the whole surface under the drop but only on the surface structure in the vicinity of the contact line. Consequently eq 3 should be modified, substituting surface fraction parameter Φ_S by a differential fraction parameter Φ_D, which corresponds to the solid−liquid surface fraction for an infinitesimal displacement ε of the contact line. For $\varepsilon \rightarrow 0$, it yields the linear fraction parameter Φ_L which is the linear surface fraction along the contact line (Figure 2). Due to interface pining and deformation, Φ_L (or Φ_D) is no longer constant but changes according to contact line position as depicted in Figure 2. This consideration adds a coupled variable to eq 3 and thus leads to eq 5 in which the two extremum values of Φ_L associated with θ_A and θ_R yield advancing and receding ACA

$$\cos\theta_C^* = \Phi_L(1+\cos\theta_Y) - 1 \qquad (5)$$

This model is more complex than the classical view because, except for particular cases, Φ_L or Φ_D cannot be easily calculated or observed. In ref 31, theoretical values of Φ_D are approximated to predict advancing and receding angles of water and decane on simple patterns such as stripes, rings, or spirals.

Our method consists of testing various liquids on a single kind of pattern (mushroom-like structures) of varying Φ_S. From the measured advancing and receding angles, we extract experimental values of Φ_L (maximum and minimum values corresponding to the advancing and receding angle, respectively). We eventually investigate the evolution of $\Phi_{L,MAX}$ and $\Phi_{L,MIN}$ according to Φ_S and compare the results to theoretical prediction reported in ref 31.

Furthermore, differential or linear surface fraction parameter is probably dependent on θ_Y. Up to now, the problem of coupling between Φ_L or Φ_D and θ_Y is not explicitly questioned in the literature. We suppose here that Φ_L mostly depends on microstructures geometry and hardly on θ_Y and, thus, that the deformation of the contact line is quite similar for different liquids on a given microstructure geometry. This point will be developed in the Results and Discussion section with regard to the experimental results.

This so-called 1D model of wetting is of great importance with regard to CAH on microstructured surfaces. Indeed using eq 3 which considers Φ_S as a constant, CAH is given by eq 6. Since $\Phi_S < 1$, hysteresis is decreased compared to a smooth surface. However, considering variable parameter Φ_L, hysteresis is given by eq 7. In this case, the Cassie state does not necessarily reduce

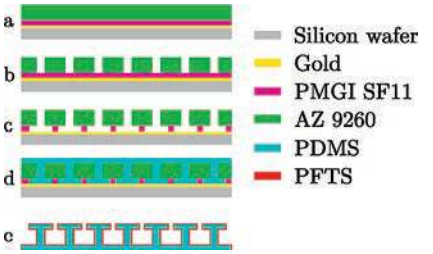

Figure 3. Main steps used for the fabrication of mushroom-like microstructures on PDMS: (a) PMGI and AZ9260 spin-coating, (b) photolithography of AZ9260, (c) etching of PMGI, (d) molding and curing of PDMS, and (e) release and PFTS coating.

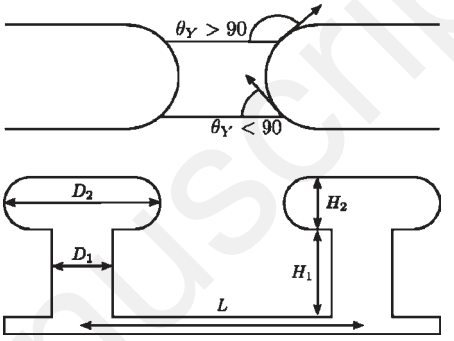

Figure 4. Microstructures' dimensions and contact line pining on the upper side of the cap for $\theta_Y > 90°$ and on the lower part for $\theta_Y < 90°$.

the hysteresis. It depends on the extreme values of Φ_L according to contact line pining at the leading and trailing edges of the droplet

$$\cos\theta_{C,R}^* - \cos\theta_{C,A}^* = \Phi_S(\cos\theta_R - \cos\theta_A) \qquad (6)$$

$$\cos\theta_{C,R}^* - \cos\theta_{C,A}^* = \Phi_{L,max}(1+\cos\theta_R) - \Phi_{L,min}(1+\cos\theta_A) \qquad (7)$$

Materials and Methods

Mushroom-like microstructured surfaces are fabricated by molding polydimethylsiloxane (PDMS) onto a patterned sacrificial photoresist bilayer.[32] For the mold AZ9260 (MicroChemicals) is used as a thick photoresist and PMGI SF11 (MicroChem) as an undercut layer. Sylgard 184 PDMS was purchased from Down Corning (Midland, U.S.A.), mixed with curing agent at a ratio of 10:1 wt %, and degassed for 30 min before spin-coating onto the mold.

The fabrication steps are listed in Figure 3. First, a gold layer is sputtered on a 3 in. silicon wafer, forming a low adhesion surface for the base of the mold. Then PMGI and AZ9260 resists are spin-coated to thicknesses which define structures cap thickness H_2 and height H_1 (Figures 3a and 4). A single photolithography step of the thick resist defines spacing L and base diameter D_1 (Figures 3b and 4). Cap diameter D_2 is obtained by etching of the undercut PMGI layer (Figures 3c and 4). To achieve a good homogeneity and reproducibility of PMGI etching, it is important to keep exactly the same protocol (same beaker and developer volume, no agitation). Moreover during prototyping, regular control of the undercut distance should be done because etch rate may also depends on thick resist patterns (L and D_1). Next, a PDMS layer is spin-coated and degassed for 15 min to ensure that it entirely fills the cavities (Figure 3d). Polymer is cured at 60 °C for 3 h, avoiding

(27) Lafuma, A.; Quere, D. *Nat. Mater.* **2003**, *2*, 457–460.
(28) Extrand, C. W. *Langmuir* **2002**, *18*, 7991–7999.
(29) Gao, L. C.; McCarthy, T. J. *Langmuir* **2009**, *25*, 14105–14115.
(30) Bormashenko, E. *Langmuir* **2009**, *25*, 10451–10454.
(31) Choi, W.; Tuteja, A.; Mabry, J. M.; Cohen, R. E.; McKinley, G. H. *J. Colloid Interface Sci.* **2009**, *339*, 208–16.
(32) Sameoto, D.; Menon, C. *J. Micromech. Microeng.* **2009**, *19*, 115002.

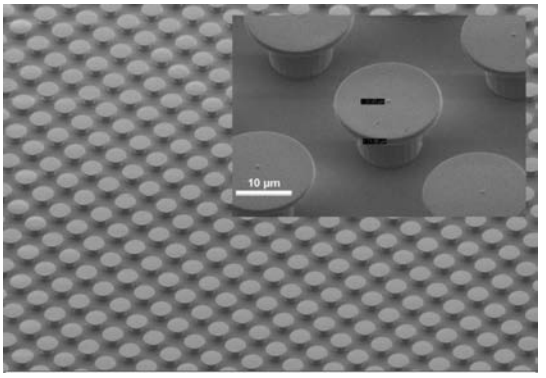

Figure 5. SEM image of a microstructured PDMS surface (SN2).

stress or mold deformation. Before demolding, a narrow strip of PDMS must be cut and peeled of around the wafer to allow solvent to access the mold. Resists are then dissolved for 10 h in Microposit remover 1165. A smaller development time (5 h) can be achieved by heating the remover; however, it induces a large absorption of solvent and dissolved resists in the polymer. A second bake step of PDMS (110 °C, 1 h in an oven) enables solvent evaporation and improves polymer strength. Finally, the resulting PDMS microstructures are functionalized with a hydrophobic monolayer: after an O_2 plasma treatment to generate silanol groups on the PDMS surface, 50 μL of perfluorodecyltrichlorosilane (PFTS) solution (10^{-3} M) are evaporated onto the surface under vacuum. Although smooth PDMS is already hydrophobic, PFTS presents a lower CAH and reduces PDMS swelling when exposed to low surface tension liquids.

Figure 5 shows a SEM image of a PDMS microstructured surface. Height H_1 and cap thickness H_2 are set from AZ9260 and PMGI layers thicknesses to 8 and 1.5 μm, respectively. Spacing L is fixed to 30 or 40 μm by a photolithography mask. The base diameter D_1 is fixed to 10 μm, and the cap diameter D_2 ranges from 20 to 30 μm, depending on undercut layer etching time. In Table 1 are summarized the different configurations investigated in this work and the corresponding surface fraction Φ_S, ranging from 0.2 to 0.8. Due to the limited resolution of the fabrication process (~0.3 μm), structures can be slightly different from the target design. However, the technique enables rapid prototyping using conventional photolithography. We achieved samples with a total thickness (microstructures + PDMS supporting layer) ranging from 100 μm to several millimeters, depending on spin speed of PDMS. The thinnest samples have been successfully handled without being damaged and can be transferred on any solid surface.

Superomniphobic surfaces have been characterized using a drop shape analysis system (DSA100, Krüss GmbH, Germany). It consists of an automated tilting table which incorporates a light source, a CDD camera (50 frames/s), and an automatic dosing system. A drop is deposited onto the surface, and then the tilting table rotates from 0 to 90° (by step of 0.3° every 0.3 s) while drop deformation and contact angle variations are recorded every 20 ms. This configuration corresponds to 16 measurements for one unique angle up to the sliding angle. Before sliding we assume to be in a quasi static state. Static ACA is measured just after drop deposition, while advancing and receding angles are measured just before contact lines depining during tilting. A ±1° error is assumed on CA computation and each measurement is operated 5 times.

It is to be noted that the rotation axis of the tilting table and the optical axis (corresponding to CDD camera) are the same. Thus on the images and video taken, the surface appears horizontal while the droplet shape is deformed. Different liquids have been tested owing to their surface tension from 72.2 mN/m for water down to 27.5 mN/m for hexadecane (Table 2). For high surface tension liquids such as water and glycerol, it can be difficult to differentiate Wenzel and Cassie states because both lead to similar static ACA. However, the light diffraction below the drop and lower CAH allow us to ensure that the drop is in a Cassie configuration.

Table 1. Spacing and Cap Diameter, and the Corresponding Surface Fraction Parameter Φ_S for the Investigated Samples[a]

sample	spacing, L (μm)	cap diameter, D_2 (μm)	$\Phi_S = \pi(D_2/2)^2/L^2$
SN1	30	21	0.35
SN2	40	21	0.20
SN3	40	25	0.30
SN4	30	28	0.60
SN5	30	31	0.84

[a] Values for cap diameter D_2 are measured by optical microscopy and averaged over 5 different structures.

Table 2. Different Liquids Used and Their Surface Energy

liquid	surface energy (mN/m)
deionized water	72.2
glycerol	64.0
CH2I2	50.8
BF2	42.0
NTF2	32.0
hexadecane	27.5

Results and Discussion

Wetting properties characterization of these surfaces has been made by the tilting method. Because the value of static angles strongly depends on the deposition method, we focus on advancing and receding angles which are more reproducible for a more rigorous characterization of the surface properties. Figure 6 illustrates the variation of the receding angle of a 8 μL glycerol droplet on surface 3 (SN3, Φ_S = 0.3) while the table is continuously tilting at 0.3° every 0.3 s. The first part of the curve indicates a continuous decrease of the ACA, due to the gravity and corresponding to a quasi static state. The hysteresis is calculated just before the first contact line jump (tilting angle = 18.3°). CAH is the difference between the minimum receding angle (red star in Figure 6) and the maximum advancing angle (variation not shown here). The latter reaches its maximum at the leading edge of the drop and shows hardly variations after advancing line depining. It is to be noted that advancing and receding ACA are not necessarily captured at the same time because depining of advancing and receding edges does not occur simultaneously. Hysteresis mainly comes from the resistance at the trailing edge,[33] consequently the advancing line depins first, leading to drop elongation and deformation, and then the receding line depins which yields to drop sliding. As soon as the drop begins to slide on the surface, a dynamic phenomenon starts and a closer look at the receding edge reveals contact line jumps from one microstructure to the other (Figure 6).

Figure 7 displays static, receding and advancing ACA obtained on sample SN3 in Table 1. This surface, as all the other ones tested, is able to support a metastable Cassie state with a static apparent CA around 145° for different liquids with surface energy ranging from 72.2 to 27.5 mN/m (see Table 2). For all tested samples and liquids, despite of the large static angle, a large hysteresis is observed, as shown in Figure 7 for sample SN3. This behavior, not paradoxical to a Cassie state, was expected and can be explained by strong contact line pining at the trailing edge of the drop, as explained in the Introduction.

(33) Reyssat, M.; Quere, D. *J. Phys. Chem. B* **2009**, *113*, 3906–3909.

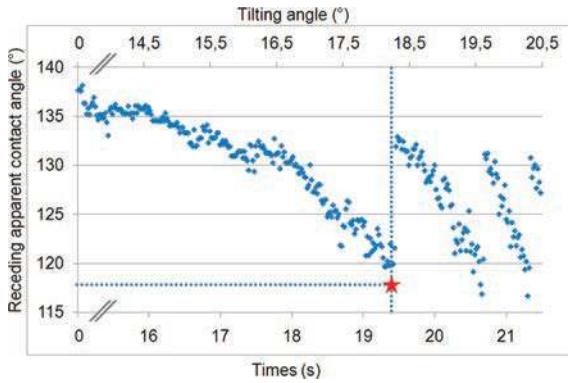

Figure 6. Variation of the receding angle for a 8 μL glycerol droplet on a tilting microstructured PDMS surface (1°/s). Red star corresponds to the considered receding ACA.

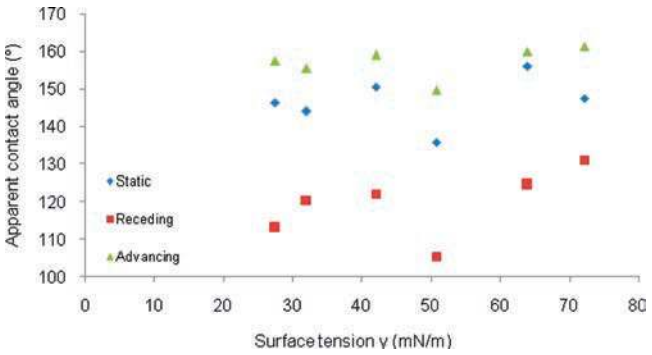

Figure 7. Static, receding, and advancing apparent contact angles according to liquid surface tension (sample 3).

It is to be noted that the investigated surfaces were not able to support a metastable state with other liquids such as methanol, isopropanol, or acetone ($\gamma \approx 23$, 23, and 25.2 mN/m respectively). In that case energy barrier between metastable Cassie and stable Wenzel configuration might be too low and easily overcome by capillary pressure or weak external perturbations (i.e., thermal fluctuations, capillary waves, etc.). Moreover important surface deformation is observed as soon as these solvents penetrate the microstructures, although their swelling ratio is rather low (1.02, 1.09, and 1.06, respectively[34]). This could be explained by the increased liquid−solid contacting surface in the Wenzel state which might intensify the swelling effect. Due to the complex shape of the microstructures, swelling could also results in some strain, amplifying surface deformation. Eventually, swelling effect cannot be considered as responsible for the failure of the composite interface, indeed swelling ratio of hexadecane is equals to 1.14[35] and does not prevent the Cassie configuration. In that case slight deformation is observed due to swelling of the structure's cap above contact line position. A solution to overcome swelling phenomena would be to add an insulating layer between the PDMS and the PFTS coating.

In order to confront the high experimental CAH to the linear fraction parameter Φ_L along the contact line (as previously presented in Introduction), advancing and receding apparent angles (for the same sample SN3) have been connected to the corresponding advancing and receding angles on a smooth surface (Figure 8). We compare first these results to the classical Cassie−Baxter model (eq 3) and observe a significant deviation

(34) Lee, J. N.; Park, C.; Whitesides, G. M. *Anal. Chem.* **2003**, *75*, 6544–6554.
(35) Dangla, R.; Gallaire, F.; Baroud, C. N. *Lab on a Chip* **2010**, http://pubs.rsc.org/en/Content/ArticleLanding/2010/LC/C003504A.

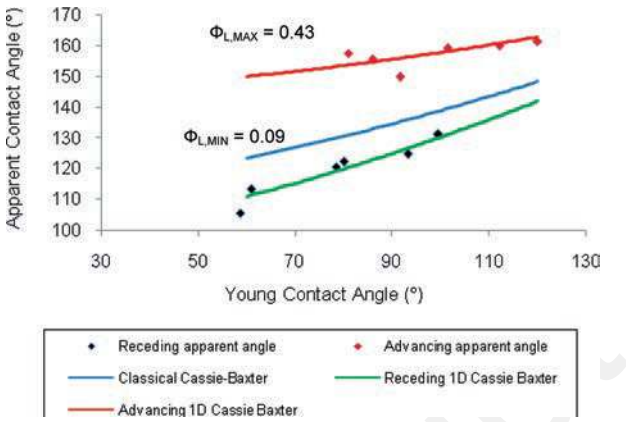

Figure 8. Results for sample number 3 ($\Phi_S = 0.3$). Experimental advancing and receding apparent contact angles as a function of experimental advancing and receding angles on a smooth surface. Results differ from the classical Cassie model (considering Φ_S constant). Fitting of 1D Cassie model gives an approximation of extremum values of Φ_L.

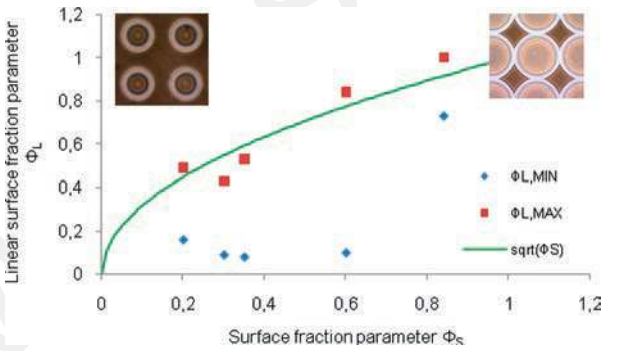

Figure 9. Maximum and minimum linear fraction parameter as a function of surface fraction parameter. The green line represents the model of Choi et al.[31]

(blue line in Figure 8). Assuming the linear Cassie model, we then fit eq 5 to these results to obtain an estimation of the maximum and minimum values of Φ_L, considering advancing and receding apparent angles, respectively. In the case of sample 3 ($\Phi_S = 0.3$), a minimum value of Φ_L is found to be 0.09, and a maximum to be 0.43.

This method is repeated over 5 different samples. For each one, a series of measurements using 6 different liquids allow us to estimate the maximum and minimum values of Φ_L. Results are reported in Figure 9. $\Phi_{L,MAX}$ and $\Phi_{L,MIN}$ are represented as a function of Φ_S (red squares and blue diamonds, respectively). We also plot the theoretical model of Choi et al.[31] which predicts $\Phi_{L,MAX} = \sqrt{\Phi}$ (green curve) and $\Phi_{L,MIN} = 0$ on a discrete hoodoo surface. The model for $\Phi_{L,MAX}$ is in good agreement with our experimental results. Concerning $\Phi_{L,MIN}$, it remains constant around 0.1 for the samples (1−4 in Table 1), which is close to the expected value. Concerning sample 5 ($\Phi_S = 0.84$), $\Phi_{L,MIN}$ clearly diverges from the predicted value. This is most likely due to the different geometry of sample 5 in the sense that structures' caps are next to each other (right insert in Figure 9) as compared to samples 1−4 for which structures are separated (left insert in Figure 9). This changes the advancing contact line behavior and results in a smaller ACA and consequently higher $\Phi_{L,MIN}$. Thus the surface comes close to a smooth surface for which $\Phi_{L,MIN} = \Phi_{L,MAX} = \Phi_S$. Up to now, we were not able to design samples with Φ_S below 0.2 because as spacing L becomes too large, the composite interface tends to fail easily for low surface

tension liquids. A solution would be to scale down the geometry of the pattern that is hard to achieve with our molding process.

Conclusion

We have presented in this paper an approach to design sticky superomniphobic surfaces on a flexible and transparent PDMS substrate. The surfaces are able to support a metastable Cassie state with a wide range of liquids (surface energies ranging from 72.2 to 24 mN/m). Despite the large apparent static contact angles measured on these surfaces, they also exhibit large contact angle hysteresis, which is in contradiction with the widespread idea that Cassie state reduces hysteresis. This behavior is explained considering the 1D model of wetting for which apparent contact angles are related to linear surface fraction of liquid − solid contact along the contact line rather than to surface fraction of solid − liquid contact under the drop. A comparison of our results with the theoretical prediction of Choi et al. confirms the 1D wetting model. Moreover, a single couple of values ($\Phi_{L,MIN}$ and $\Phi_{L,MAX}$) has been extracted from various liquids on a given surface. It points out the low dependence of Φ_L parameter on the liquid used. However, this coupling of variables in the modified Cassie equation remains to be rigorously investigated by observation of contact line deformation and pining under the drop by a more sensitive imaging characterization.

Acknowledgment. We thank the "Direction Générale de l'Armement" for financial support and Christophe Boyaval for SEM characterizations.